The sign of electron g-factor in $GaAs_{1-x}N_x$ measured by using the Hanle effect

V K Kalevich, E L Ivchenko, A Yu Shiryaev, M M Afanasiev and A Yu Egorov

A.F. Ioffe Physico-Technical Institute, St. Petersburg 194021, Russia

M Ikezawa and Y Masumoto

Institute of Physics, University of Tsukuba, Tsukuba 305-8571, Japan

E-mail: kalevich@solid.ioffe.ru

Abstract. Positive signs of the effective g-factors for free electrons in the conduction band and electrons localized on deep paramagnetic centers have been measured in nitrogen dilute alloy $GaAs_{0.979}N_{0.021}$ at room temperature. The g-factor signs have been determined from an asymmetry in the depolarization of edge photoluminescence in a transverse magnetic field (Hanle effect) at the oblique incidence of the exciting radiation and oblique-angle detection of the luminescence. The tilted spin polarization of free electrons is induced under interband absorption of circularly polarized light, and the paramagnetic centers acquire spin polarization because of spin-dependent capture of free spin-polarized electrons by these centers. The measured Hanle curve is a superposition of two lines, narrow and broad, with the widths ~ 400 G and ~ 50000 G, arising due to the depolarization of localized and free electrons, respectively. The difference in the linewidths by two orders of magnitude strongly indicates much longer spin lifetime for the paramagnetic centers as compared with that for the free carriers. The magnitude and direction of the asymmetry in the measured Hanle curve have been found to depend on the partial contributions to the recombination radiation from the heavy- and light-hole subbands split by a uniaxial deformation of the $GaAs_{1-x}N_x$ film grown on a GaAs substrate. We have extended the theory of optical orientation in order to calculate the excitation spectrum of the photoelectron tilted-spin polarization and the circularly-polarized luminescence spectrum taking into account that, in the strained samples under study, the light-hole subband lies above the heavy-hole one. The results have further been used to calculate the shape of Hanle curve as a function of the excitation and registration energies as well as the incidence and detection angles and to compare the theory with experiment.

1. Introduction

Dilute III-N-V alloys with the group-V cations partially substituted by nitrogen, e.g., GaAsN and InGaAsN, have recently attracted particular attention owing to a number of their unusual properties. Thus, an increase of nitrogen content in the alloy is accompanied by an anomalous reduction of the fundamental band gap, by more than 0.1 eV per 1% of N as the nitrogen concentration increases from zero up to 4% [1, 2, 3, 4], as well as by a drastic increase of the electron effective mass and enhanced nonparabolicity of the Γ_6 conduction band [5, 6, 7, 8] (for reviews, see also [9, 10]). These specific properties are related to the N-substitution-induced resonant electronic states within the conduction band continuum and an anticrossing of the localized nitrogen states with the extended conduction states of the semiconductor matrix [11, 12, 13]. Qualitatively, the available experimental data are consistent with the simple phenomenological band anticrossing (BAC) model which takes into account the anticrossing hybridization only with the levels of isolated (single) nitrogen atoms [11]. As a result, the two hybridized conduction bands, E_+ and E_-, are formed. As the nitrogen concentration increases, the lower band, E_-, shifts down in energy reducing the fundamental energy-band gap E_g. Simultaneously, the band-bottom effective mass becomes heavier and the nonparabolicity coefficient rises considerably.

The band-structure modification involves a remarkable change in the gyromagnetic factor, g, of electrons in the conduction band E_- [14, 15]. The change is caused by two reasons. Firstly, as in the case of conventional alloys $In_xGa_{1-x}As$ [16, 17], the band-gap shrinkage leads to a monotonous downward shift of the effective g-factor below the value of g-factor in GaAs matrix ($g = -0.44$ in GaAs at helium temperature) [14]. Secondly, the coupling with isolated nitrogen levels, with the Landé factor being positive and close to the electron g-factor in vacuum $g_0 = 2$, tends to shift the g value upwards, as it has been first found experimentally in InGaAsN when studying the dependence of the absorption coefficient on the magnetic field [14]. The two effects have opposite signs and partially compensate each other. The BAC model predicts an initial growth in the dependence $g(x)$ [14]. The dependence is smooth and, as calculated for $GaAs_{1-x}N_x$ in [15], it has a maximum value $g \approx 0$ at $x \sim 1\%$. At the same time, detailed measurement and comparison of the left- and right-circularly polarized photoluminescence spectra performed in $GaAs_{1-x}N_x$ in a longitudinal magnetic field at helium temperature for $x \leq 0.6\%$ have shown that g grows sharply with increasing x, reverses its sign from negative to positive at $x \approx 0.04\%$, reaches a value of 0.7 in the range $x = 0.04 \div 0.1\%$ and retains that value with small deviations as x increases up to 0.6% [15]. Such an abrupt dependence of g on x at small x has been interpreted in terms of a modified $\mathbf{k} \cdot \mathbf{p}$ model [13, 15]. This model takes into account the hybridization of the host conduction band not only with the localized levels due to single N atoms but also with the levels which are formed by clusters of N atoms, pairs and triplets, and lie closer to the conduction-band bottom.

The data on the g-factor in $GaAs_{1-x}N_x$ with high nitrogen concentration are highly

desirable for the purpose of checking various theoretical models. However, to the best of our knowledge, such experimental data for $x > 0.6\%$ are lacking.

In the present work the sign of the electron g-factor in the $GaAs_{1-x}N_x$ conduction band has been measured at room temperature for $x = 2.1\%$. To this end, we used the dependence of the sign of the asymmetry of Hanle effect of optically spin-polarized electrons, measured under oblique excitation, on the g-factor sign. This method is based on the relationship between the direction of Larmor precession of electron spin in a magnetic field and the g-factor sign. As compared to other methods, this method is advantageous for studying crystals with high nitrogen content, particularly at high (up to room) temperatures when the photoluminescence occurs over a broad spectrum. The fundamentals of the method are presented in Section 3, together with the discussion of peculiarities of the electron spin polarization and the oblique Hanle effect caused by the splitting of the Γ_8 valence band due to a uniaxial strain of the GaAsN films grown on GaAs substrates.

Section 4 provides the theory extended in order to calculate the magnitude and orientation of photoelectron spin polarization, the circular polarization of photoluminescence and the Hanle-curve shape as a function of the energy of absorbed and emitted photons in a uniaxially strained semiconductor with the top of the light-hole subband to be higher in energy than the top of the heavy-hole subband.

In the GaAsN alloys under study, the optical spin polarization of conduction electrons at room temperature has been found to be anomalously high [4, 18]. This is the result of spin-dependent recombination of polarized conduction electrons on deep paramagnetic centers which apparently appear during the introduction of nitrogen atoms into GaAs. The capture of free electrons is accompanied by efficient dynamic spin polarization of electrons bound on the centers. In its turn, the polarized centers kinetically affect the polarization of free electrons so that a strongly coupled spin system of free and localized electrons is formed. A change in the polarization of localized electrons manifests itself in a remarkable change of the free-electron polarization. Thus, from the analysis of the curve of magnetic depolarization of the interband photoluminescence contributed by free particles, one can determine the g-factor signs of both free and bound electrons. In Section 5 we present experimental results together with the results of numerical calculation taking into account the influence of spin-dependent recombination on the electron spin polarization.

2. Samples and experimental details

We studied the undoped 0.1 μm-thick $GaAs_{0.979}N_{0.021}$ layer grown by rf-plasma-assisted solid-source molecular-beam epitaxy at 350–450°C on semi-insulating (001) GaAs substrate [4]. The nitrogen content and crystallinity of the grown layer were examined by x-ray diffraction technique. The as-grown structure was annealed for 5 min at 700°C in a flow of arsenic in the growth chamber. Continuous-wave tunable Ti:sapphire laser was used for photoluminescence (PL) excitation. Spin polarization of electrons was created

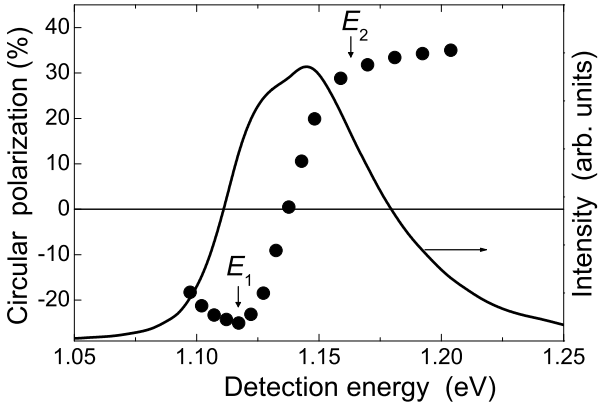

Figure 1. Spectral dependencies of the PL intensity (solid curve) and of the PL circular polarization degree (circles) for the $GaAs_{0.979}N_{0.021}$ layer under normal incidence ($\theta = 0$) of the pump beam and detection of the PL. Excitation energy $\hbar\omega_{\rm exc} = 1.312\,$eV. Arrows indicate the PL detection energies $E_1 = 1.117$ and $E_2 = 1.163$ at which the Hanle curves presented in Fig. 2 are measured.

upon the interband absorption of circularly polarized light [19]. It was monitored by measuring the degree of circular polarization of PL, defined as $\rho = (I^+ - I^-)/(I^+ + I^-)$, where I^+ and I^- are the right (σ^+) and left (σ^-) circularly polarized PL components. The value ρ and PL intensity in a wavelength range up to $1.4\,\mu$m were measured using a high-sensitive polarization analyzer [20] comprising a quartz polarization modulator [21], a lock-in two-channel photon counter, and a photomultiplier with an InGaAsP photocathode. The measurements were carried out at 300 K.

Figure 1 shows the spectra of PL intensity (solid curve) and of PL circular polarization degree (circles) measured in $GaAs_{0.979}N_{0.021}$ layer under normal incidence of the pump beam and the detection of luminescence along the growth axis. The PL spectrum consists of two strongly overlapping inhomogeneously broadened bands where the low-energy PL band is negatively polarized (relative to the polarization of the exciting beam), whereas the high-energy band is polarized positively. As we have shown earlier [4], the two PL bands appear due to splitting of the light- and heavy-hole valence subbands induced by uniaxial compression along the growth axes of $GaAs_{1-x}N_x$ film grown on GaAs substrate. In its turn, this compression arises from large lattice mismatch between the film and substrate. The crystal splitting of the PL bands, Δ_c, increases with increase of the nitrogen content and at $x = 2.1\%$ equals 29 meV. An interrelation of the sign of the PL circular polarization and the type of recombination transition in $GaAs_{1-x}N_x$ is considered in detail in [4]. Under simultaneous excitation of electrons from both valence subbands, realized in Fig. 1, the negative and positive PL polarizations are due to recombination of conduction electrons with the light and heavy holes, respectively. Since under an uniaxial compression the top of the light-hole subband is situated above the top of the heavy-hole subband [22], the low-energy PL band is polarized negatively.

In bulk semiconductor, the spin relaxation rate of conduction electrons grows

dramatically with temperature and decreases electron polarization down to units and fractions of % at room temperature [19]. At the same time, the absolute values both of negative and positive polarization in Fig. 1 reach $30 \div 35\%$, which is near to the maximal magnitude of 50% determined by selection rules. Such anomalous enhancement of free electron polarization in GaAsN is due to dynamic polarization of electrons bound on deep paramagnetic centers [18, 23, 24]. The paramagnetic centers arise with an incorporation of nitrogen in GaAs and are polarized as a result of spin-dependent capture on them of the polarized conduction electrons. The polarized centers increase the free electron polarization which can reach $\approx 100\%$ at strong pumping.

3. The Hanle effect in GaAsN alloys

3.1. Electron Hanle effect under normal excitation and detection

The Hanle effect is a depolarization of photoluminescence by a magnetic field $\boldsymbol{B}$ directed perpendicular to continuous-wave pump beam [19]. The effect originates from Larmor precession of electron spins, which destroys their polarization. In the simplest case, Hanle effect is described by Lorentzian $\rho(B)/\rho(B=0) = 1/(1+B^2/B_{1/2}^2)$ with half-width at half maximum, $B_{1/2} = \hbar/g\mu_B T_s$, where g is the electron Landé g-factor, μ_B is the Bohr magneton, and T_s is the electron spin-polarization lifetime. Figure 2 shows the Hanle curves measured in $GaAs_{0.979}N_{0.021}$ for the positive (a) and negative (b) PL polarization under the normal incidence of pump light onto the sample and the detection of the PL in the opposite direction (backscattering configuration). The measurements were carried out with the energy of the excitation quantum $\hbar\omega_{\rm exc} = 1.312\,$eV, at which the conduction electrons are excited from both valence subbands. One can see that for both positive and negative PL polarization the Hanle curve is superimposition of the narrow and wide curves with the half-widths being different by two orders of magnitude. A qualitative explanation of such a complex shape of the $\rho(B)$ dependency is the following. Spin lifetime of electrons bound on paramagnetic centers, T_{sc}, can exceed spin lifetime of free electrons, T_s, by orders of magnitude at room temperature. Therefore, the half-width of Hanle curve of bound electrons, $B_{1/2}^c = \hbar/g_c\mu_B T_{sc}$ (here g_c is the gyromagnetic g-factor of bound electrons), should be far less than the half-width of Hanle curve of free electrons $B_{1/2}$. As noted above, the spin-dependent recombination results in formation of a strongly coupled spin-system of free and bound electrons, where a variation of the polarization of the centers is accompanied by change in the free-electron polarization. Due to this, the $\rho(B)$ curve is the sum of two curves with strongly different half-widths, where the narrow curve describes the Hanle effect of bound electrons and the wide curve presents depolarization of free electrons. Solid curves in Fig. 2 are calculated using the equation $\rho(B) = \rho_0/[1+(B/B_{1/2})^2] + \rho_{0c}/[1+(B/B_{1/2}^c)^2] + \rho_{\rm res}$ at $B_{1/2} = 25000\,$G and $B_{1/2}^c = 185\,$G. It is seen that the calculated curves describe reasonably the measured ones in Fig. 2 for both positive and negative polarization. During the calculation the fitting parameters were ρ_0, ρ_{0c} and $\rho_{\rm res}$. At present, the

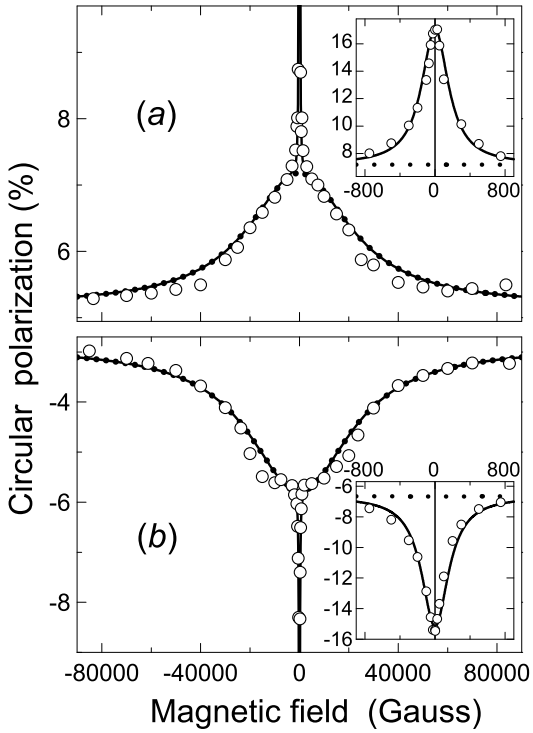

Figure 2. Experimental Hanle curves (open circles) measured in $GaAs_{0.979}N_{0.021}$ at excitation and detection along the normal to the sample. Excitation energy $\hbar\omega_{\rm exc} = 1.312\,$eV, detection energy $\hbar\omega_{\rm det}$ is equal to $E_2 = 1.163\,$eV (a) and $E_1 = 1.117\,$eV (b). Solid curves are superpositions of the calculated Hanle curves for free (dotted curves) and bound electrons (see text for details). Inserts show the initial parts of the Hanle curves in the range of small magnetic fields.

origin of the constant polarization $|\rho_{\rm res}| \sim 4\%$ is not clear and additional studies should be done for its elucidation.

3.2. Electron Hanle effect under oblique excitation and detection

The Hanle effect can provide measuring the sign of the Landé g-factor of electrons [25, 26, 27] since a rotation direction of mean electron spin in a magnetic field depends on the g-factor sign. The most suitable way to find the g-factor sign is to use a specular geometry of experiment. In this geometry, the exciting light falls on the sample obliquely, the luminescence is detected at an angle to the exciting beam while a magnetic field is perpendicular to both the excitation and detection directions, and lies in the crystal surface plane [26], as shown in Fig. 3.

In specular geometry, the dependence $\rho(B)$ in bulk zinc-blende semiconductor has the form [26]:

$$\frac{\rho(B)}{\rho_0} = \frac{\cos\alpha + \varphi\sin\alpha}{1+\varphi^2} \quad , \tag{1}$$

where α is the angle between the directions of excitation and detection, ρ_0 is the degree of polarization for $B = 0$ and $\alpha = 0$, $\varphi = \Omega T_s = g\mu_B B T_s/\hbar$ is the angle through which

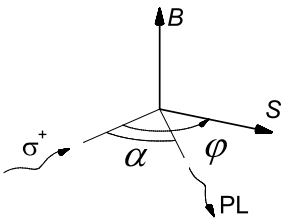

Figure 3. Experimental configuration for the g-factor sign measurements. The angle α is the angle between the excitation beam and the direction of the detected photoluminescence.

the mean spin $\boldsymbol{S}$ of electrons with the g-factor equal to g turns during the electron spin lifetime $T_s = \tau\tau_s/(\tau + \tau_s)$, τ and τ_s are the electron lifetime and spin relaxation time in the conduction band, $\boldsymbol{\Omega} = g\mu_B\boldsymbol{B}/\hbar$ is the Larmor frequency, and the Born magneton $\mu_B > 0$. Equation (1) was derived taking into account the fact that in a bulk unstrained GaAs-type crystal the mean electron spin in the moment of creation, $\boldsymbol{S}_0$, is parallel to the exciting beam, and the degree of PL polarization is equal to the projection of $\boldsymbol{S}$ on the direction of detection: $\rho = \boldsymbol{S}\boldsymbol{n}_1$, where $\boldsymbol{n}_1$ is the unit vector along the direction of registration [19, 28]. At $\alpha = 0$, the Hanle curve is a symmetrical function on magnetic field as, for example, one can see in Fig. 2. For $\alpha \neq 0$, the $\rho(B)$ plot is not symmetrical with respect to the $B = 0$ point. The value of ρ is larger for the magnetic field direction at which the electron spin precesses toward the luminescence observation axis. Note, that for measuring the g-sign it is sufficient to record the asymmetry in the dependence of the absolute value of ρ on B.

The above method acquires distinctive features [27] if the heavy and light hole subbands are split due to the uniaxial deformation in a bulk crystal or due to quantum-size effect in a nanostructure.

First, in this case the direction of the mean spin of photogenerated electrons $\boldsymbol{S}_0$ may not coincide with the direction of the exciting beam. Theory [28] (see also [29]) developed for uniaxially strained crystals yields the following expressions for the mean spins of the electrons created with $\boldsymbol{k} \approx 0$ from states close to the tops of light-hole ($lh \to c$ transition) and the heavy-hole ($hh \to c$ transition) subbands:

$$\boldsymbol{S}_{0lh} = \frac{3(\boldsymbol{\nu}\boldsymbol{n}_0)\boldsymbol{\nu} - 2\boldsymbol{n}_0}{5 - 3(\boldsymbol{\nu}\boldsymbol{n}_0)^2}, \qquad \boldsymbol{S}_{0hh} = \frac{-\boldsymbol{\nu}(\boldsymbol{\nu}\boldsymbol{n}_0)}{1 + (\boldsymbol{\nu}\boldsymbol{n}_0)^2} \quad , \tag{2}$$

where $\boldsymbol{\nu}$ and $\boldsymbol{n}_0$ are unit vectors along the deformation (growth) axis and pump beam direction. As seen from Eqs. (2), the spin $\boldsymbol{S}_{0hh}$ is parallel to the deformation axis for any light incidence angle, whereas the angle between $\boldsymbol{S}_{0lh}$ and $\boldsymbol{\nu}$ is twice the angle θ between the excitation direction and the growth axis (Fig. 4) [30]. The light-hole and heavy-hole splitting can be neglected if the energy of the photogenerated holes exceeds substantially the splitting energy Δ_c [28]. Such situation can be realized when $\hbar\omega_{\rm exc} - E_g \gg \Delta_c$, where E_g is the forbidden gap of the deformed crystal. In this case, the electrons are excited from both valence subbands, and, as in a bulk unstrained crystal, their mean spin $\boldsymbol{S}_{0\Sigma}$ is directed along the exciting beam: $\boldsymbol{S}_{0\Sigma} \downarrow\uparrow \boldsymbol{n}_0$ (Fig. 4). Thus, with the increase of

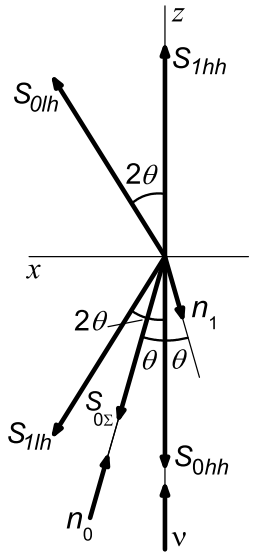

Figure 4. Scheme of orientation of spins $\boldsymbol{S}_{0hh}$, $\boldsymbol{S}_{0lh}$, $\boldsymbol{S}_{0\Sigma}$ and vectors $\boldsymbol{S}_{1hh}$, $\boldsymbol{S}_{1lh}$ with respect to the directions $\boldsymbol{n}_0$ of excitation, $\boldsymbol{n}_1$ of detection and $\boldsymbol{\nu}$ of deformation ($\boldsymbol{\nu}$ is a perpendicular to the sample surface) in the case of specular configuration.

excitation energy from $\hbar\omega_{\rm exc} \approx E_g$ towards $\hbar\omega_{\rm exc} \gg E_g + \Delta_c$, the spin $\boldsymbol{S}_0$ changes from $\boldsymbol{S}_{0lh}$ to $\boldsymbol{S}_{0\Sigma}$ rotating counterclockwise through angle $(180^\circ - 3\theta)$.

Second, in the case of valence-subband splitting, the PL polarization is determined by projection of $\boldsymbol{S}$ not on the direction of observation $\boldsymbol{n}_1$, as this should be for a bulk unstrained semiconductor, but rather on the vector $\boldsymbol{S}_1$, which depends on the angle between $\boldsymbol{n}_1$ and $\boldsymbol{\nu}$ vectors and on the actual recombination energy [28, 19]:

$$\rho = -4\boldsymbol{S}\boldsymbol{S}_1 \ . \tag{3}$$

For recombination with the tops ($\boldsymbol{k} \approx 0$) of the light-hole and heavy-hole subbands, the vectors $\boldsymbol{S}_{1lh}$ and $\boldsymbol{S}_{1hh}$ are given by the same expressions (2) as $\boldsymbol{S}_{0lh}$ and $\boldsymbol{S}_{0hh}$, but with $\boldsymbol{n}_0$ being replaced by $\boldsymbol{n}_1$. We readily see that $\boldsymbol{S}_{1hh}$ is always parallel to the growth axis, while $\boldsymbol{S}_{1lh}$ is at an angle 2θ to this axis (Fig. 4). If the PL detection energy $\hbar\omega_{\rm det} \approx E_g$, recombination with the light-holes is only possible and, therefore, $\boldsymbol{S}_1 = \boldsymbol{S}_{1lh}$. When $\hbar\omega_{\rm det} - E_g \gg \Delta_c$, the crystal valence-band splitting can be ignored and an effective direction of the PL detection, given by vector $\boldsymbol{S}_1$, coincides with the real one: $\boldsymbol{S}_1 \downarrow\uparrow \boldsymbol{n}_1$. So, with increase of the detection energy, the vector $\boldsymbol{S}_1$ changes its direction from $\boldsymbol{S}_{1lh}$ to $(-\boldsymbol{n}_1)$, rotating clockwise through angle $(180^\circ - 3\theta)$.

Since both the value and direction of the $\boldsymbol{S}_0$ and $\boldsymbol{S}_1$ vectors are energy dependent, the Hanle curves will be different for different excitation and detection energies. However, as shown in [27], they can still be described by Eq. (1), provided the angle α is replaced by the angle $(\gamma - \beta)$, where γ and β are the angles between the z axis and vectors $\boldsymbol{S}_1$ and $\boldsymbol{S}_0$, respectively, reckoned counterclockwise from the z axis.

4. Theory

The above qualitative analysis of orientation of the vectors $\boldsymbol{S}_0, \boldsymbol{S}_1$ and the angle between them is based on Eqs. (2) valid for the Γ-point, $\boldsymbol{k} = 0$. The values of $\boldsymbol{S}_0$ and $\boldsymbol{S}_1$ for arbitrary frequencies $\hbar\omega_{\rm exc}$ and $\hbar\omega_{\rm det}$ can be found taking into account the interband optical transitions with $\boldsymbol{k} \neq 0$ where the heavy- and light-hole states are mixed. Such kind of calculations has been performed for unstrained bulk zinc-blende-lattice semiconductors [29], strained bulk semiconductors with the top of the heavy-hole subband lying above that of the light-hole subband [31, 32], quantum-well structures in the approximation of infinitely-high barriers [33] and for finite barriers [34] (see also [35]), and semiconductor superlattices [36].

In this section we will follow the method of Ref. [31] developed in order to calculate the optical orientation of electron spins under interband absorption of circularly polarized light normally incident on a hexagonal crystal, e.g., CdS or CdSe. In fact, in [31] the quasicubic model of the valence band structure is used: the crystal splitting of the higher two valence subbands is obtained by applying an effective uniaxial strain to a crystal of the cubic symmetry with the Γ_8 valence band. Here we generalize the approach of Ref. [31] to consider (i) the oblique incidence of the exciting light on the sample, and (ii) the opposite sign of the uniaxial strain resulting in the opposite sequence of the split subbands, now the light-hole subband lies above the heavy-hole subband.

The spin-polarized electrons are described by the spin-density matrix $f_{ss'}$, where $s, s' = \pm 1/2$ are the spin indices. This matrix can be found from the balance matrix equation

$$\left\{\frac{\partial \hat{f}}{\partial t}\right\}_{\rm spin.rel.} + \left\{\frac{\partial \hat{f}}{\partial t}\right\}_{\rm Larmor} = \dot{\hat{f}}\,, \tag{4}$$

where the first and second terms describe the spin relaxation and Larmor precession of the electron spins, and the right-hand side term is the generation rate of the electron spin-density matrix. Four components of the latter matrix can be calculated by using the general equation

$$\dot{f}_{ss'} \propto \sum_{\boldsymbol{k}n} \delta[E_c(\boldsymbol{k}) - E_{v_n}(\boldsymbol{k}) - \hbar\omega] \sum_j M_{cs,v_nj}(\boldsymbol{k}) M^*_{cs',v_nj}(\boldsymbol{k})\,. \tag{5}$$

Hereafter we omit common multipliers and use the following notations: $\boldsymbol{k}$ is the electron wave vector, $E_c(\boldsymbol{k})$ and $E_{v_n}(\boldsymbol{k})$ are the electron energies in the conduction band c and the valence subband $v_n (n = \pm)$ given by

$$E_c(\boldsymbol{k}) = E_0 + \frac{\hbar^2 k^2}{2m_c}\,,\; E_{v_n}(\boldsymbol{k}) = Ak^2 - \frac{\Delta_c}{2} \pm R\,, \tag{6}$$

$$R = \sqrt{\left(\frac{\Delta_c}{2}\right)^2 + B^2k^4 + \frac{B\Delta_c}{2}(3k_z^2 - k^2)}\,,$$

z is the uniaxial-strain axis coinciding with the crystal growth axis, the index $j = 1, 2$ enumerates degenerate states in the v_+ and v_- valence subbands; m_c is the electron

effective mass in the conduction band, A and B are the standard valence-band parameters entering the Luttinger Hamiltonian taken in the spherical approximation ($D = \sqrt{3}B$); Δ_c is the splitting of the Γ_8 valence band at $\boldsymbol{k} = 0$ called the crystal splitting. In the following we assume a value of Δ_c to be positive in which case the indices v_+ and v_- correspond to the light-hole and the heavy-hole subbands, respectively, and the parameter E_0 coincides with the fundamental band gap E_g. The opposite order of the light- and heavy-hole subbands considered in Ref. [31] is described by negative values of Δ_c. The matrix elements for interband electron transitions, $M_{cs,v_nj}(\boldsymbol{k})$, are related to the interband matrix elements of the momentum operator $\hat{\boldsymbol{p}}$ by

$$M_{cs,v_nj}(\boldsymbol{k}) \propto \boldsymbol{e} \cdot \boldsymbol{p}_{cs,v_nj}(\boldsymbol{k}) \,,$$

where $\boldsymbol{e}$ is the light polarization unit vector.

Under oblique incidence with the incidence plane containing the axes x and z (and perpendicular to the y axis) the initial spin $\boldsymbol{S}_0$ of the photogenerated electrons is related to $\dot{\hat{f}}$ by

$$S_z = \frac{1}{2}\,\frac{\dot{f}_{\frac{1}{2},\frac{1}{2}} - \dot{f}_{-\frac{1}{2},-\frac{1}{2}}}{\dot{f}_{\frac{1}{2},\frac{1}{2}} + \dot{f}_{-\frac{1}{2},-\frac{1}{2}}} \,,\; S_x = \frac{\mathrm{Re}\{\dot{f}_{\frac{1}{2},-\frac{1}{2}}\}}{\dot{f}_{\frac{1}{2},\frac{1}{2}} + \dot{f}_{-\frac{1}{2},-\frac{1}{2}}} \,. \tag{7}$$

One can show that the sum over j in Eq. (5) can be reduced to

$$\sum_j M_{cs,v_nj}(\boldsymbol{k}) M^*_{cs',v_nj}(\boldsymbol{k}) \propto (\hat{D}\hat{U}_n\hat{D}^\dagger)_{ss'} \,, \tag{8}$$

where $\hat{D}$ is the 2×4 matrix of the interband matrix elements $\langle \Gamma_6, s|\boldsymbol{e}\cdot\hat{\boldsymbol{p}}|\Gamma_8, m\rangle$ ($s = 1/2, -1/2; m = 3/2, 1/2, -1/2, -3/2$) calculated between the Γ_6 conduction and Γ_8 valence Bloch functions:

$$D_{sm} = \frac{p_{cv}}{\sqrt{6}} \begin{bmatrix} -\sqrt{3}e_+ & 2e_z & e_- & 0 \\ 0 & -e_+ & 2e_z & \sqrt{3}e_- \end{bmatrix} ,$$

$e_\pm = e_x \pm \mathrm{i}e_y$, p_{cv} is the interband matrix element $\langle S|\hat{p}_z|Z\rangle$ with S and Z being the standard orbital Bloch functions at the Γ point,

$$\hat{U}_n = \frac{\mathcal{H}(\boldsymbol{k}) - E_{v_{\bar{n}}}(\boldsymbol{k})}{E_{v_n}(\boldsymbol{k}) - E_{v_{\bar{n}}}(\boldsymbol{k})} \quad (\bar{n} \neq n) \,,$$

$\mathcal{H}(\boldsymbol{k})$ is the effective electron Hamiltonian in the valence band Γ_8 split into two subbands of the heavy and light holes.

Since the matrices $\hat{D}, \hat{D}^\dagger$ and the electron energy spectrum are independent of the wave-vector azimuth angle $\varphi_{\boldsymbol{k}}$ the Hamiltonian $\mathcal{H}(\boldsymbol{k})$ in $\hat{U}_n$ can be averaged over $\varphi_{\boldsymbol{k}}$ and reduced to a diagonal matrix. We omit the further details and present the final result for the generation matrix (5) written as a sum of the partial contributions $\dot{f}^{(n)}_{ss'}$ due to the optical transitions from the subbands v_n.

The partial contributions $\dot{f}^{(n)}_{ss'}$ can eventually be presented in the form

$$\dot{f}^{(n)}_{ss'} = W_n\delta_{ss'} - \frac{\rho^0}{2}(V^{(n)}_x \sin\theta\ \sigma_x + V^{(n)}_z \cos\theta\ \sigma_z) \,, \tag{9}$$

where ρ^0 is the degree of circular polarization of the light wave in vacuum, θ is the refraction angle, σ_x and σ_z are the Pauli spin 2×2 matrices. The other notations are defined by

$$W_n = Z_n \frac{t_s^2 + t_p^2}{2} + \frac{n}{4} F(\theta) Z'_n \,,$$

$$V_z^{(n)} = t_s t_p (Z_n + n Z'_n) \,,\; V_x^{(n)} = t_s t_p (Z_n - \frac{n}{2} Z'_n) \,,$$

$$F(\theta) = \frac{1}{4}(2t_s^2 - t_p^2 + 3t_p^2 \cos 2\theta) \,,$$

t_s and t_p are the amplitude transmission coefficients of the s- and p-polarized light,

$$Z_n \propto 4\pi \int\limits_0^{+\infty} k^2 dk \int\limits_0^{\pi} \sin\theta_{\boldsymbol{k}} d\theta_{\boldsymbol{k}} \delta[E_c(\boldsymbol{k}) - E_{v_n}(\boldsymbol{k}) - \hbar\omega] \,, \tag{10}$$

$$Z'_n \propto 4\pi \int\limits_0^{+\infty} k^2 dk \int\limits_0^{\pi} \sin\theta_{\boldsymbol{k}} d\theta_{\boldsymbol{k}} \frac{Bk^2(1 - 3\cos^2\theta_{\boldsymbol{k}}) - \Delta_c}{R} \delta[E_c(\boldsymbol{k}) - E_{v_n}(\boldsymbol{k}) - \hbar\omega]. \tag{11}$$

Note that Z_n is proportional to the reduced density of states "conduction band - valence subband n".

The integrals (10) and (11) can be readily calculated assuming

$$\eta = \frac{|B|}{(\hbar^2/2m_c) + |A|} \ll 1 \,.$$

In GaAs the dimensionless parameter η is about 0.23. For the light propagating in the direction $\boldsymbol{n} = (\sin\theta, 0, \cos\theta)$ one has

$$W_+ = \sqrt{\chi_+} \left[\frac{t_s^2 + t_p^2}{2} - \frac{1}{2}\, \Pi(\chi_+) F(\theta) \right] \,,$$

$$W_- = \begin{cases} 0 & \text{for} \quad 1 > \varepsilon > 0 \,, \\ \sqrt{\chi_-} \left[\frac{t_s^2 + t_p^2}{2} + \frac{1}{2}\, \Pi(\varepsilon_-) F(\theta) \right] & \text{for} \quad \varepsilon > 1 \,. \end{cases}$$

Here

$$\chi_+ = \eta\varepsilon \,,\; \varepsilon = \frac{\hbar\omega - E_g}{\Delta_c} \,,$$

$$\chi_- = \begin{cases} 0 & \text{for} \quad 1 > \varepsilon > 0 \,, \\ \eta(\varepsilon - 1) & \text{for} \quad \varepsilon > 1 \,, \end{cases}$$

ω is the light frequency, and the function Π of a variable X is defined by

$$\Pi(X) = \frac{1}{4} \left(\frac{3 + 2X - 4X^2}{\sqrt{6X}} \arcsin \sqrt{\frac{6X}{1 + 4X^2 + 2X}} + |1 - 2X| \right) \,. \tag{12}$$

The photoelectron average spin components in the directions z and x are determined by

$$S_z = \frac{1}{2}\rho^0 t_s t_p \cos\theta \frac{R_z^+ + R_z^-}{W_+ + W_-}\,, \qquad (13)$$
$$S_x = \frac{1}{2}\rho^0 t_s t_p \sin\theta \frac{R_x^+ + R_x^-}{W_+ + W_-}\,,$$

where

$$R_z^+ = -\frac{1}{2}\sqrt{\chi_+}\,[1 - 2\Pi(\chi_+)]\,,\; R_x^+ = -\frac{1}{2}\sqrt{\chi_+}\,[1 + \Pi(\chi_+)]\,,$$

$R_z^- = R_x^- = 0$ if $1 > \varepsilon > 0$, and

$$R_z^- = -\frac{1}{2}\sqrt{\chi_-}\,[1 + 2\Pi(\chi_-)]\,,\; R_x^- = -\frac{1}{2}\sqrt{\chi_-}\,[1 - \Pi(\chi_-)]\,,$$

if $\varepsilon > 1$.

The above equations correspond to positive Δ_c. However, they are also valid for negative Δ_c if the function (12) is replaced by

$$\Pi(X) = -\frac{1}{4}\left(1 + 2X + \frac{3 - 2X - 4X^2}{\sqrt{6X}} \ln\frac{1 + 2X + \sqrt{6X}}{\sqrt{1 + 4X^2 - 2X}}\right)\,.$$

The angle φ between the vector of the average spin and the axis z equals to

$$\varphi = \arctan\left(\frac{R_x}{R_z}\tan\theta\right) + (1 - \mathrm{sign}\{S_z\})\;\frac{\pi}{2} \qquad (14)$$
$$\approx \arctan\left(\frac{R_x}{R_z}\theta\right) + (1 - \mathrm{sign}\{S_z\})\;\frac{\pi}{2}\,,$$

where $R_z = R_z^+ + R_z^-, R_x = R_x^+ + R_x^-$. Here we take into account that, in the medium with a big index of refraction, the refraction angle θ is small even for remarkable incidence angles.

Under photoexcitation near the fundamental edge, $\hbar\omega \approx E_g$, one has $\chi_- = 0$, $W_- = 0$ and the optical transitions are allowed only from the upper light-hole subband. For $0 < \varepsilon = (\hbar\omega - E_g)/\Delta_c \ll 1$, the function $\Pi(\chi_+)$ in (12) tends to 1, and according to Eq. (13) the ratio S_x/S_z is given by $-2\tan\theta$ and φ by $-\arctan(2\tan\theta)$ in agreement with the first equation (2). At the edge of the transitions from the heavy-hole subband, $\varepsilon - 1 = (\hbar\omega - E_g - \Delta_c)/\Delta_c \ll 1$, the function $\Pi(\chi_-) \to 1$ and, therefore, $R_x^- \to 0$ and R_z^- is negative. Therefore, for electrons excited from the top of the v_- subband, $\varphi \to \pi$, in agreement with the second equation (2).

5. Calculation, experimental results and discussion

5.1. Specular configuration

It is convenient to use the reduced excitation and detection energies $\varepsilon_{\mathrm{exc}} = (\hbar\omega_{\mathrm{exc}} - E_g)/\Delta_c$ and $\varepsilon_{\mathrm{det}} = (\hbar\omega_{\mathrm{det}} - E_g)/\Delta_c$. Our measurements have been made for a large excitation energy $\varepsilon_{\mathrm{exc}} = 7.2$ permitting the crystal splitting of the valence subbands to be neglected. Below we present the results of calculation for that energy. They show

that in this case $\beta \approx 180^\circ - \theta$, i.e. $\boldsymbol{S}_0 \downarrow\uparrow \boldsymbol{n}_0$, and $|\boldsymbol{S}_0| = 0.25\cos\theta \approx 0.25$, which is in full agreement with the above qualitative analysis based on the expressions (2).

The dependencies of the polarization $\rho(0) = \rho_0\cos(\gamma-\beta)$ and of the angle $(\gamma-\beta)$ on the detection energy $\varepsilon_{\rm det}$ calculated for zero magnetic field and specular configuration are shown by solid lines in Fig. 5a and Fig. 5c. One can see that for the detection energy $\varepsilon_{\rm det} = 0$, when recombination with the light holes with $k = 0$ is only possible and the vector $\boldsymbol{S}_1$ is directed at the angle $\gamma = 180^\circ - 2\theta$ to the z axis, the angle $(\gamma-\beta) = -\theta$ and polarization $\rho(0) \approx -0.5$. In this case, $|\boldsymbol{S}_1| = 0.5$. When increasing $\varepsilon_{\rm det}$, the admixture of the heavy-hole states leads to the increase of $\rho(0)$ and $(\gamma-\beta)$. These changes of $\rho(0)$ and $(\gamma-\beta)$ are small when $\varepsilon_{\rm det}$ varies from 0 to 1. However, the $\rho(0)$ and $(\gamma-\beta)$ dependencies have abrupt humps at $\varepsilon_{\rm det} = 1$, when the transitions from the heavy-hole subband are switched on, involving the creation of electrons with opposite signs. With further increase of $\varepsilon_{\rm det}$, the quantity $\rho(0)$ increases rapidly, then reverses its sign from negative to positive and approaches its maximal value $\rho(0) = 0.25$ at $\varepsilon_{\rm det} \approx 2$, while the angle $(\gamma-\beta)$ approaches the maximal value of $(-180^\circ + 2\theta)$, corresponding to which are $\gamma = \theta$ and $|\boldsymbol{S}_1| = 0.25$. Those values of $\rho(0)$ and $(\gamma-\beta)$ remain practically invariable with $\varepsilon_{\rm det}$ increasing still further.

The angle $(\gamma-\beta) = -90^\circ$ ($\boldsymbol{S}_1 \perp \boldsymbol{S}_0$) when the detection energy is equal to $\varepsilon_\perp$ (shown by a vertical dashed line in Fig. 5). Therefore at such an energy of detection the dependence of $\rho(0)$ on $\varepsilon_{\rm det}$ passes through zero, although $|S_1(\varepsilon_\perp)| \neq 0$ (see thick solid line in Fig. 5b). Note that $|S_1(\varepsilon_\perp)| = 0$ only when the direction of PL detection coincides with the axis of strain ($\boldsymbol{n}_1 \parallel \boldsymbol{\nu}$, $\theta = 0$) (thin solid line in Fig. 5b).

Since $\cos(\gamma-\beta)$ and $\sin(\gamma-\beta)$ reverse their signs as the argument changes by 180°, the $(\gamma-\beta)$ angle can be substituted by the angle α, which, as shown in Fig. 5d, is approximately equal $-\theta$ at $\varepsilon_{\rm det} < 1$, 2θ at $\varepsilon_{\rm det} > 2$ and changes drastically within the range $1 < \varepsilon_{\rm det} < 2$, making a leap from -90° to +90° at $\varepsilon_{\rm det} = \varepsilon_\perp$ ($\varepsilon_\perp \approx 1.09$). With such definition of angle α, expression (1) for the Hanle effect takes the form:

$$\rho(B) = \rho_0 \frac{\cos\alpha + \varphi\sin\alpha}{1+\varphi^2}\mathrm{sign}(\varepsilon_{\rm det} - \varepsilon_\perp) \quad , \tag{15}$$

where $\rho_0 = 4|S_0||S_1|T_s/\tau$.

We consider the coupled spin-system of free and bound electrons in the model of spin-dependent recombination proposed by Weisbuch and Lampel [37], applied by Paget [38] and generalized in [18]. In this model the magnetic-field dependence of the PL polarization can be with high accuracy described by two Lorentzians:

$$\rho(B) = \left[\rho_0 \frac{\cos\alpha + \varphi\sin\alpha}{1+\varphi^2} + \rho_{0c}\frac{\cos\alpha + \varphi_c\sin\alpha}{1+\varphi_c^2} + \rho_{\rm res}\right]\mathrm{sign}(\varepsilon_{\rm det} - \varepsilon_\perp)\,, \tag{16}$$

where the first and the second term in the square brackets describe depolarization of the free and the bound electrons, respectively, $\varphi_c = g_c\mu_B B T_{sc}/\hbar$ is the angle of rotation of the mean spin of localized electrons $\boldsymbol{S_c}$ in a magnetic field $\boldsymbol{B}$ during the lifetime of their spin T_{sc}, $\rho_{\rm res}$ is the residual polarization, observed experimentally in high magnetic field.

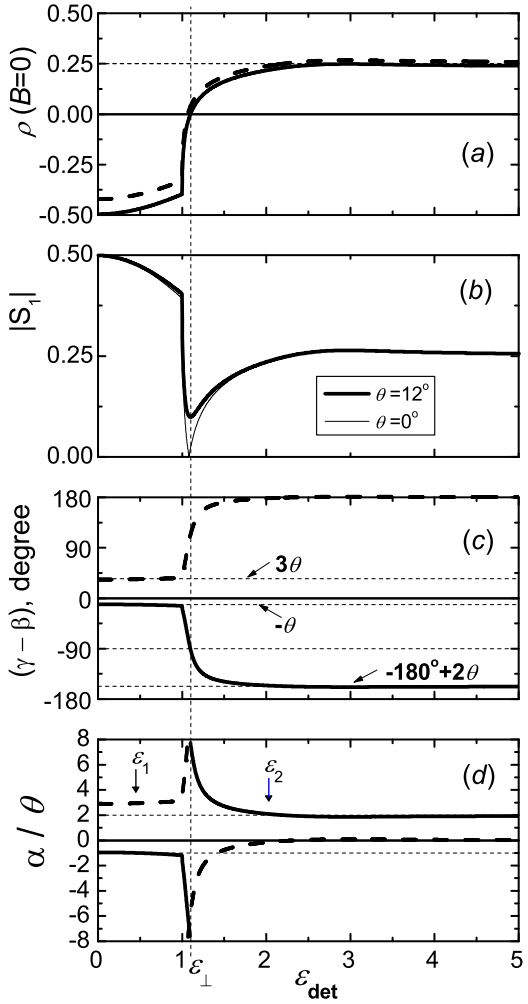

Figure 5. The PL circular polarization (a), the spin $|S_1|$ (b), the angles $(\gamma - \beta)$ (c) and α (d) calculated as a function of the PL detection energy for specular (solid) and backscattering (dashed) configurations for the refraction angle $\theta = 12°$, corresponding to the incidence angle of 48°, and excitation energy $\varepsilon_{\rm exc} = 7.2$ in the absence of magnetic field. In b, the dependence $|S_1(\varepsilon_{\rm det})|$ is shown also for the normal incidence, $\theta = 0$. In the case of specular configuration the normal to the sample surface coincides with the bisectrix between the exciting beam and the direction of the PL detection.

It is convenient to measure signs of g and g_c at $\varepsilon_{\rm det} \gg 1$ and $\varepsilon_{\rm det} \ll 1$. As seen from Fig. 5d, in the first case $\alpha = +2\theta$ (as in bulk unstrained semiconductor), and in the second case $\alpha = -\theta$.

High energy detection ($\alpha = +2\theta$)

We realized the first case at $\varepsilon_{\rm det} = \varepsilon_2 = 2.03$ (here, just as in all the following measurements, $\varepsilon_{\rm exc} = 7.2$ and the refraction angle $\theta = 12°$). The experimental Hanle curve (open circles in Fig. 6) has a manifestly asymmetric shape in this case. The maximum of its narrow part (Fig. 6a), which corresponds to depolarization of bound electrons, shifts to positive values of the magnetic field. For the employed specular geometry of experiment, to this corresponds the positive sign of g_c [18] (note that

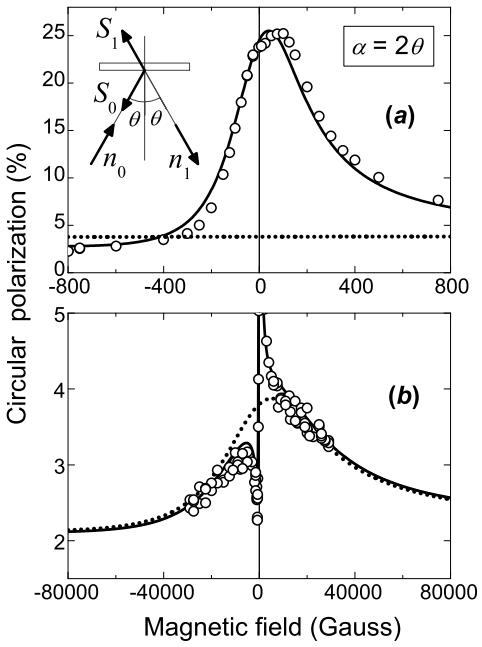

Figure 6. Experimental (circles) and calculated (solid, dotted) Hanle curves obtained in $GaAs_{0.979}N_{0.021}$ in the specular configuration set-up at high-energy excitation and high-energy recombination when $\alpha \approx 2\theta$. $\hbar\omega_{\rm exc} = 1.312\,$eV, $\hbar\omega_{\rm det} = E_2 = 1.163\,$eV, $\theta = 12^\circ$. Inset illustrates relative orientation of the spins $\boldsymbol{S}_0$, $\boldsymbol{S}_1$ and the unit vectors $\boldsymbol{n}_0$, $\boldsymbol{n}_1$.

the Hanle curve, measured in the same geometry in bulk GaAs, in which $g < 0$, has a maximum at $B < 0$). The maximum of the broad part of the experimental curve $\rho(B)$ determined by depolarization of free electrons is less pronounced, since it is superimposed by the depolarization curve of bound electrons, which has a greater-by-an-order amplitude in zero magnetic field. The polarization of bound electrons, however, decreases rapidly as the magnetic field increases, and we can neglect its contribution at $|B| > 15\,$kG. The solid curve in Fig. 6 is calculated from Eq. (16) with the same values of depolarization curve halfwidths for bound and free electrons $B^c_{1/2} = 185\,$G and $B_{1/2} = 25000\,$G that have been obtained from the fitting of the experimental Hanle curves in Fig. 2, measured under normal excitation and detection (the same values $B^c_{1/2}$ and $B_{1/2}$ will be used below in approximation of experimental Hanle curves measured under different experimental conditions). One can see that this curve approximates the experimental dependence $\rho(B)$ satisfactorily. This makes it possible to extract the partial Hanle curve for free electrons that is described by the first term in Eq. (16) and shown by the dotted line in Fig. 6. As the dotted line has a maximum at $B > 0$ (Fig. 6b), we can conclude that $g > 0$.

Low energy detection ($\alpha = -\theta$)

The experimental dependence $\rho(B)$ for this case that has been realized at $\varepsilon_{\rm det} = 0.45$, is shown by open circles in Fig. 7. The negative sign of the measured luminescence polarization results from the fulfillment of the condition $\varepsilon_{\rm det} < \varepsilon_\perp$. Solid curve in Fig. 7

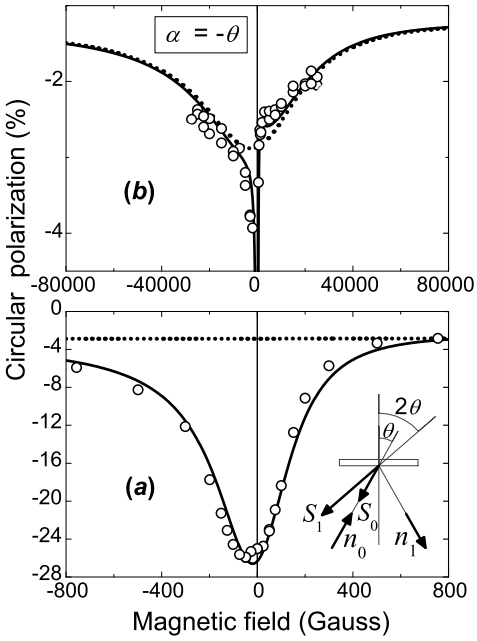

Figure 7. Experimental (circles) and calculated (solid, dotted) Hanle curves obtained in $GaAs_{0.979}N_{0.021}$ in the specular configuration at high-energy excitation and the electron recombination with the light holes when $\alpha \approx -\theta$. $\hbar\omega_{\rm exc} = 1.312\,$eV, $\hbar\omega_{\rm det} = E_1 = 1.117\,$eV, $\theta = 12^\circ$.

is calculated using Eq. (16) for $\alpha = -\theta$. The maxima (in the absolute value) on the depolarization curves for the bound (Fig. 7a) and free (dotted line in Fig. 7b) electrons are situated at $B < 0$, which also attests to positive signs of g and g_c.

5.2. Backscattering configuration

Deformation-induced splitting of the light- and heavy-hole subbands allows the Hanle curve asymmetry to be observed even in the backscattering configuration where the directions of detection and excitation are antiparallel, $\boldsymbol{n}_1 \downarrow\uparrow \boldsymbol{n}_0$. To realize that possibility, the magnetic field $\boldsymbol{B}$, lying in the sample surface plane, is directed perpendicular to the exciting beam, while the sample is turned around vector $\boldsymbol{B}$ in such a way that there is nonzero angle θ between the normal to the sample (axis $\boldsymbol{\nu}$) and the exciting beam (vector $\boldsymbol{n}_0$), as shown in the insert in Fig. 8.

The dependence of angle α between vectors $\boldsymbol{S}_0$ and $\boldsymbol{S}_1$ on detection energy $\varepsilon_{\rm det}$ calculated for backscattering configuration and $\varepsilon_{\rm exc} = 7.2$ is shown by dashed line in Fig. 5d. One can see that $\alpha = +3\theta$ if $\varepsilon_{\rm det} < 1$ and $\alpha \approx 0$ if $\varepsilon_{\rm det} > 2$.

Low energy detection ($\alpha = +3\theta$).

At $\varepsilon_{\rm det} < 1$ angle $\alpha \approx 3\theta$, which makes the asymmetry of the experimental Hanle curve (open circles in Fig. 8) more pronounced than in the case of the specular configuration when $\alpha \approx -\theta$. The negative sign of polarization is due to the fact that $\varepsilon_{\rm det} < \varepsilon_\perp \approx 1.07$. Solid and dotted curves in Fig. 8 are calculated from Eq. (16) and the second term of Eq. (16), respectively, for $\alpha = 3\theta$. It is seen that the maxima

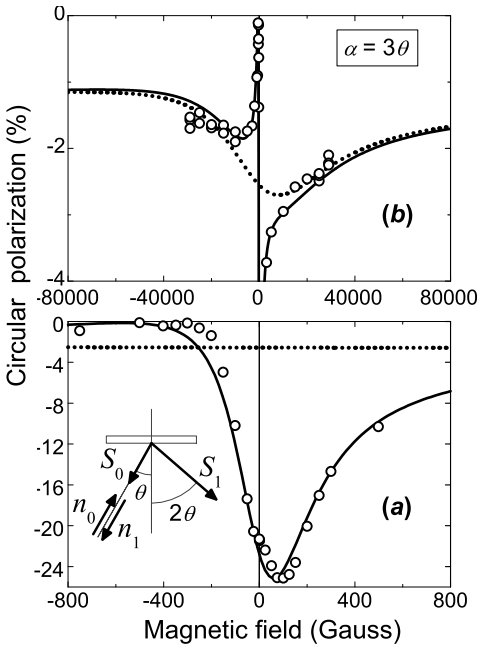

Figure 8. Experimental (circles) and calculated (solid, dotted) Hanle curves obtained in $GaAs_{0.979}N_{0.021}$ in the backscattering configuration at high-energy excitation and the electron recombination with light holes when $\alpha \approx 3\theta$. $\hbar\omega_{\rm exc} = 1.312\,$eV, $\hbar\omega_{\rm det} = E_1 = 1.117\,$eV, $\theta = 12^\circ$.

of depolarization curves both for the bound (Fig. 8a) and the free electrons (dotted line in Fig. 8a) are found in the region of positive values of the magnetic field. For a backscattering configuration this indicates that the signs of g and g_c, which is in full agreement with the result obtained with the use of specular configuration.

High energy detection ($\alpha = 0$).

At $\varepsilon_{\rm det} > 2$ (when deformation splitting can be neglected) the angle $\alpha \approx 0$ and, according to Eq. (16), the Hanle curve must be symmetrical and insensitive to the sign of g-factor. Indeed, the experimental Hanle (open circles in Fig. 9), measured at $\varepsilon_{\rm det} = \varepsilon_2 = 2.03$, is symmetric.

The experimental dependencies $\rho(B)$ presented above have been measured under high-energy excitation ($\varepsilon_{\rm exc} \gg 1$) and detection energy $\varepsilon_{\rm det} \gg 1$ or $\varepsilon_{\rm det} < 1$, when angle α remains practically invariable with varying $\varepsilon_{\rm det}$. Under these conditions the greatest absolute value of the angle α and, respectively, the greatest asymmetry of Hanle curve are observed in specular configuration at $\varepsilon_{\rm det} \gg 1$ ($\alpha = 2\theta$) and in backscattering configuration at $\varepsilon_{\rm det} < 1$ ($\alpha = 3\theta$). A greater asymmetry of Hanle curve can be obtained in specular configuration under excitation and detection with only a light hole participating ($\varepsilon_{\rm det} < \varepsilon_{\rm exc} < 1$), when $\alpha = -4\theta$ [27]. Note that the maximum asymmetry of Hanle curve can be realized both in specular and backscattering configurations under high-energy excitation and detection energy $\varepsilon_{\rm det} = \varepsilon_\perp$, when in the absence of magnetic field the vectors $\boldsymbol{S}_1$ and $\boldsymbol{S}_0$ are perpendicular to each other (angle $|\gamma - \beta| = 90^\circ$) and $\rho \propto \boldsymbol{S_0 S_1} = 0$, while in a magnetic field $\rho \propto \pm|S_0||S_1|\varphi/(1+\varphi^2)$, where the sign $+(-)$

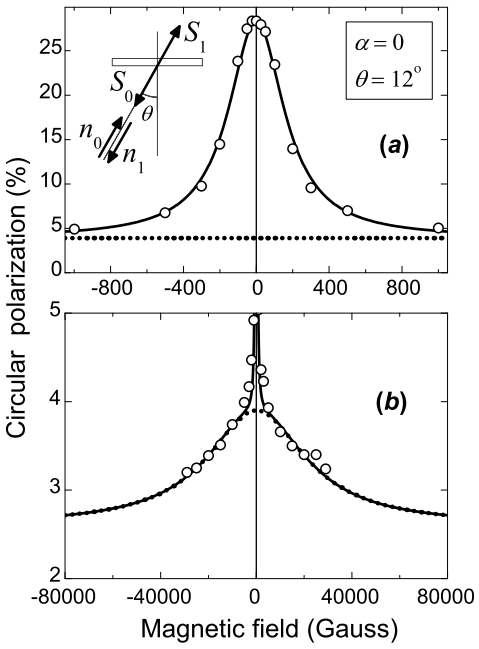

Figure 9. Experimental (circles) and calculated (solid, dotted) Hanle curves for $GaAs_{0.979}N_{0.021}$ in the case of backscattering configuration at high-energy excitation and high-energy recombination when $\alpha = 0$. $\hbar\omega_{\rm exc} = 1.312\,$eV, $\hbar\omega_{\rm det} = E_2 = 1.163\,$eV, $\theta = 12°$.

before the right-hand side corresponds to the specular (backscattering) configuration. However, at $\varepsilon_{\rm det} = \varepsilon_\perp$ the modulus of $\boldsymbol{S}_1$ vector diminishes sharply and is near zero if the refraction angle does not exceed a few degrees ($|S_1(\varepsilon_\perp)| = 0$ for $\theta = 0$), amounting to ≈ 0.1 only at angles θ close to the maximum value ($\theta_{\rm max} = 16°$ in GaAs [30]) (see Fig. 5b).

Experimental dependencies $\rho(B)$ measured in GaAsN consist of narrow and broad parts. The large amplitude of the narrow part bears witness to strong polarization of bound electrons, arising due to spin-dependent recombination. We have approximated the experimental curves $\rho(B)$ by sum of two Lorentzians, one of which describes the depolarization of bound electrons, and the other, that of free electrons. At the same time, we have shown in Ref. [18] that the polarizations of free and bound electrons are summed up additively ($\rho \propto S + S_c$) only in the limit of low polarization of bound electrons. If polarization of bound electrons is strong, it becomes necessary to solve a system of nonlinear equations, coupling polarizations of free and bound electrons [18]. As the preliminary analysis shows, in that case a substantially better fit of the experimental Hanle curve is obtained for the region of low magnetic fields, where the polarization of bound electrons dominates. The detailed theoretical description of the compound Hanle effect under an arbitrary polarization (100% including) of bound electron will be presented in a separate publication. Here we note that the shape of Hanle curves (in particular their asymmetry), obtained from the solution of a system of nonlinear equations does not differ qualitatively from the results of approximation by

two Lorentzians, which makes it possible to employ the latter for determination of the signs of g and g_c.

6. Summary

In order to determine the sign of the electron g factor in a semiconductor film, we have applied the method based on analysis of the asymmetrical Hanle effect under oblique incidence of the exciting light onto the sample and detection of the photoluminescence at oblique emission. The relationship between the g factor sign and direction of the asymmetrical shift of the Hanle curve is governed by the valence band structure, particularly, by its splitting due to an internal uniaxial strain in the film, and depends on the photoexcitation and photodetection energies. In the present experimental and theoretical work we have extended the method to the case where the internal strain shifts the light-hole subband upwards relative to the heavy-hole subband. The interband optical orientation of electron spins, circular polarization of photoluminescence, and shape of the Hanle curve have been calculated in dependence on the energies of excitation and detection as well as on the angles of incidence and secondary emission.

The experimental study has been performed on uniaxially compressed $GaAs_{1-x}N_x$ epitaxial films. The observed Hanle effect is a result of the magnetic-field induced depolarization of the coupled system of spin-polarized free electrons and electrons bound on deep paramagnetic centers. The asymmetry of the resultant Hanle curve has been measured at room temperature under oblique incidence of the pump radiation and detection in the specular or backscattering configurations. Positive signs of the gyromagnetic g-factors of the free and bound electrons in the $GaAs_{0.979}N_{0.021}$ alloy have been deduced from comparison between experiment and theory.

Acknowledgments

We are grateful to late B.P. Zakharchenya for stimulating interest in this work and to M.M. Glazov, K.V. Kavokin and V.M. Ustinov for fruitful discussions. Partial support by the Russian Foundation for Basic Research, grants of the Russian Academy of Sciences, and TARA project of the University of Tsukuba is acknowledged.

References

[1] Weyers M, Sato M and Ando H 1992 *Japan. J. Appl. Phys.* Part 2–Letters **31** L853
[2] Bi W G and Tu C W 1997 *Appl. Phys. Lett.* **70** 1608
[3] Kondow M, Kitatani T, Larson M C, Narahara K, Uomi K and Inoue H 1998 *J. Cryst. Growth* **188** 255
[4] Egorov A Yu, Kalevich V K, Afanasiev M M, Shiryaev A Yu, Ustinov V M, Ikezawa M and Masumoto Y 2005 *J. Appl. Phys.* **98** 013539
[5] Skierbiszewski C *et al* 2000 *Appl. Phys. Lett.* **76** 2409
[6] Hai P N, Chen W M, Buyanova I A, Xin H P and Tu C W 2000 *Appl. Phys. Lett.* **77** 1843

[7] Skierbiszewski C, Perlin P, Wisniewski P, Suski T, Geisz J F, Hingerl K, Jantsch W, Mars D E and Walukiewicz W 2001 *Phys. Rev.* B **65** 035207
[8] Masia F *et al* 2006 *Phys. Rev.* B **73** 73201
[9] Henini M (ed) 2005 *Dilute Nitride Semiconductors* (Oxford: Elsevier)
[10] Erol A (ed) 2008 *Dilute III-V Nitride Semiconductors and Material Systems* (*Springer Series in Material Science* vol. 105) (Berlin: Springer)
[11] Shan W, Walukiewicz W, Ager J W III, Haller E E, Geisz J F, Friedman D J, Olson J M and Kurz S R 1999 *Phys. Rev. Lett.* **82** 1221
[12] Kent P R C and Zunger A 2001 *Phys. Rev.* B **64** 115208
[13] Lindsay A and O'Reilly E P 2004 *Phys. Rev. Lett.* **93** 196402
[14] Skierbiszewski C, Pfeffer P, Łusakowski J 2005 *Phys. Rev.* B **71** 205203
[15] Pettinari G *et al* 2006 *Phys. Rev.* B **74** 245202
[16] Hermann C and Weisbuch C 1977 *Phys. Rev.* B **15** 823
[17] Hermann C and Weisbuch C 1984 *Optical Orientation* ed Meier F and Zakharchenya B P (Amsterdam: North Holland) pp 463–508
[18] Kalevich V K, Ivchenko E L, Afanasiev M M, Shiryaev A Yu, Egorov A Yu, Ustinov V M, Pal B and Masumoto Y 2005 *Pis'ma Zh. Eksp. Teor. Fiz.* **82** 509 [2005 *JETP Lett.* **82** 455]
[19] Meier F and Zakharchenya B P (ed) 1984 *Optical Orientation* (Amsterdam: North Holland)
[20] Kul'kov V D and Kalevich V K 1980 *Prib. Tekh. Eksp.* **5** 196 [1981 *Instrum. Exp. Tech.* **24** 1265]
[21] Jasperson S N and Schnatterly S F 1969 *Rev. Sci. Instrum.* **40** 761
[22] Bir G L and Pikus G E 1974 *Symmetry and Strain-Induced Effects in Semiconductors* (New York: Wiley)
[23] Lagarde D, Lombez L, Marie X, Balocchi A, Amand T, Kalevich V K, Shiryaev A, Ivchenko E and Egorov A 2007 *Phys. Status Solidi* (a) **204** 208
[24] Kalevich V K, Ivchenko E L, Shiryaev A Yu, Egorov A Yu, Lombez L, Lagarde D, Marie X and Amand T 2007 *Pis'ma Zh. Eksp.Teor. Fiz.* **85** 208 [2007 *JETP Letters* **85** 174]
[25] Vekua V L, Dzhioev R I, Zakharchenya B P, Ivchenko E L and Fleisher V G 1974 *Zh. Eksp. Teor. Fiz.* **66** 1790 [1974 *Sov. Phys. JETP* **39** 879]
[26] Kalevich V K and Kul'kov V D 1982 *Opt. Spektrosk.* **52** 200 [1982 *Opt. Spectrosc.* (*USSR*) **52** 120]
[27] Kalevich V K, Zakharchenya B P, Kavokin K V, Petrov A V, Le Jeune P, Marie X, Robart D, Amand T, Barrau J and Brousseau M 1997 *Fiz. Tverd. Tela* **39** 768 [1997 *Phys. Solid State* **39** 681]
[28] Dyakonov M I and Perel V I 1973 *Fiz. Tekh. Poluprovodn.* **7** 2335 [1973 *Sov. Phys. Semicond.* **7** 1551]
[29] Dyakonov M I and Perel V I 1984 *Optical Orientation* ed Meier F and Zakharchenya B P (Amsterdam: North Holland) pp 11–71
[30] To be precise, $\tan\zeta = 2\tan\theta$, where ζ is the angle between $\boldsymbol{S}_{0lh}$ and $\boldsymbol{\nu}$. Since the angle θ between $\boldsymbol{n}_0$ and $\boldsymbol{\nu}$ cannot exceed 16° because of the large refractive index, approximately 3.6, of GaAs and GaAsN, we can accept $\zeta \approx 2\theta$.
[31] Bir G L and Ivchenko E L 1975 *Fiz. Tekh. Poluprovodn.* **9** 1300 [1975 *Sov. Phys. Semicond.* **9** 858]
[32] Subashiev A V, Kalevich V K, Mamaev Yu A, Oskotskii B D and Yashin Yu P 1999 *Fiz. Tekh. Poluprovodn.* **33** 1307 [1999 *Semiconductors* **33** 1182]
[33] Merkulov I A, Perel V I and Portnoi M E 1991 *Zh. Eksp. Teor. Fiz.* **99** 1202 [1991 *Sov. Phys. JETP* **72** 669]
[34] Marie X, Amand T, Barrau J, Renucci P, Lejeune P and Kalevich V K 2000 *Phys. Rev.* B **61** 11065
[35] Twardovski A and Hermann C 1986 *Phys. Rev.* B **35** 8144
[36] Subashiev A V, Gerchikov L G and Ipatov A N 2004 *J. Appl. Phys.* **96** 1511
[37] Weisbuch C and Lampel G 1974 *Solid State Commun.* **14** 141
[38] Paget D 1984 *Phys. Rev.* B **30** 931